





Research Article



Synthesis and characterization of different binary and ternary phase mixtures of mesoporous nanocrystalline titanium dioxide

N. I. Ermokhina¹ · V. V. Shvalagin¹  · N. I. Romanovska¹ · P. A. Manoryk¹ · R. Yu. Barakov^{1,2} · M. O. Kompanets^{1,3} · V. I. Sapsay⁴ · D. O. Klymchuk⁴ · A. M. Puziy⁵

Received: 18 September 2020 / Accepted: 8 March 2021 / Published online: 22 March 2021
© The Author(s) 2021 

Abstract

Different phase compositions of mesoporous nanocrystalline TiO₂ (meso-nc-TiO₂), comprised of anatase (16–100%), rutile (0–70%) and brookite (0–52%) were obtained by sol–gel synthesis with or without hydrothermal treatment (HTT) by means of titanium tetrabutoxide and dibenzo-18-crown-6 as structure-forming agent in the presence of HCl. It was shown, that small amounts of surfactant and/or lanthanum salt as well as HTT determine phase composition and texture of meso-nc-TiO₂. All samples were calcined at 500 °C and characterized by SEM, TEM, XRD and N₂-adsorption/desorption isotherms. It has been established that photocatalytic properties of almost all obtained samples significantly exceed the photocatalytic activity of Evonik P-25 TiO₂ in gas phase ethanol oxidation. The most active sample is characterized by phase composition of anatase (97%)-rutile (3%). It is obvious, that decrease of photocatalytic activity of sample was affected by decrease of anatase phase content. It was shown that the specific surface area of the sample is not a key factor affecting the activity of mixed-phase meso-nc-TiO₂ samples in the process of ethanol oxidation.

Keywords Sol–gel synthesis · Hydrothermal treatment · Mesoporous TiO₂ · Mixtures of anatase with rutile and (or) brookite · Gas-phase photocatalytic oxidation

1 Introduction

Solving the global energy problems of modern society requires the development of various areas of “green technology”. Today, in the field of semiconductor photocatalysis, TiO₂ is an undoubted leader both in terms of demand and research intensity (including the synthesis and testing of a wide range of new composite titania-based materials) due to the unique combination of its properties and, first of all, non-toxicity, chemical stability and low cost

[1–19]. The efficiency of TiO₂ photocatalyst is determined by numerous parameters: crystallinity, phase composition, crystallite size, particle morphology, porosity, developed surface area, surface organization, etc. [16, 20–24]. The classic definition of “the ideal powder should be pure, stoichiometric, dense, spheroidal, and nearly monodisperse” was made by Brinker and Scherer back in 1990 [25]. 5 years later, Antonelli and Ying [26] proposed their own method of the sol–gel synthesis of mesoporous TiO₂ with a high

Supplementary Information The online version contains supplementary material available at <https://doi.org/10.1007/s42452-021-04474-y>.

✉ V. V. Shvalagin, vitaliy.shvalagin@gmail.com; shvalagin@inphyschem-nas.kiev.ua | ¹Pisarzhevskii Institute of Physical Chemistry of the National Academy of Sciences of Ukraine, Ave. Science, 31, Kyiv 03028, Ukraine. ²Department of Physical and Macromolecular Chemistry, Faculty of Science, Charles University in Prague, Hlavova 2030, 12840 Prague 2, Czech Republic. ³L.M. Litvinenko Institute of Physical–Organic Chemistry and Coal Chemistry, 50 Kharkiv Highway, Kyiv 02160, Ukraine. ⁴Institute of Botany of the National Academy of Sciences of Ukraine, Tereshchenkivska St. 2, Kyiv 01601, Ukraine. ⁵Institute of Sorption and Endoecology Problems, National Academy of Sciences of Ukraine, General Naumov St. 13, Kyiv 03164, Ukraine.



SN Applied Sciences (2021) 3:491 | <https://doi.org/10.1007/s42452-021-04474-y>

specific surface, thereby indicating the main direction of researchers' efforts to improve TiO₂ photocatalysts.

Undoubtedly, the sol–gel template method still remains one of the most advanced methods for producing mesoporous oxides. Its combination with widely used solvo (hydro) thermal processing of an intermediate amorphous organo-inorganic product allows controlling the processes of formation of unique TiO₂ materials with a certain morphology and texture at the nanoscale level [20–41].

Hydrothermal treatment at relatively low temperatures (< 200 °C) gives the possibility to obtain highly homogeneous nanocrystalline TiO₂ powders [16, 29, 31, 35, 37, 42, 43]. However, in the process of manufacturing a highly efficient photocatalyst, the obtained powders, as a rule, require calcination at temperatures not lower than 500 °C to achieve full catalytic potential [23, 24, 29, 36, 40, 44–47].

TiO₂ exists mainly in three different crystalline forms: anatase, rutile and brookite. Anatase has the highest photoactivity [48]. However, the interest in obtaining TiO₂ nanocomposites, which consist of two or three polymorphs (relatively few works for latter), is not diminishing. The results obtained in these works sometimes lead to contradictory conclusions when comparing of the photocatalytic activity of the TiO₂ mixed-phase in various redox processes. Many authors reported that the photocatalytic activity of mixtures of TiO₂ phases in a number of processes is higher in comparison with the pure single polymorphs [14, 16, 20, 21, 24, 49–51]. It is attributed to the synergistic effect of different positions of the energy levels of different phases of titanium dioxide, which leads to the spatial separation of photogenerated charges in mixed-phase materials, decrease in the negative electron–hole recombination of charges, and increase in the activity of these materials in various redox processes [20, 31, 36, 52–58].

Earlier, under conditions of neutral hydrolysis, samples of thermally stable meso-nc-TiO₂ with a pure anatase structure were obtained [59–63], demonstrating different textures with well-defined spherical morphology (micro- and nanospheres) and a narrow pore distribution. Calcined at 500 °C after hydrothermal treatment at 175 °C TiO₂ samples had a radically more developed porous structure compared to samples without hydrothermal treatment [59]. Mesoporous hierarchical TiO₂ microspheres ranging in size from 0.6 to 3.0 μm, were formed by aggregation and agglomeration of homogeneous nanoparticles (30–70 nm), in turn formed by primary spherical particles—anatase crystallites of about 10 nm (XRD). The introduction of small amounts of surfactant and a lanthanum salt into the reaction mixture led to increase in crystallinity, change in morphology, and development of the of meso-nc-TiO₂ texture. Spherical particles of micrometer scale

in the presence of La³⁺ ions are not formed. It should be emphasized that anatase is the only crystalline phase (in the absence of signs of phase transformation) of meso-nc-TiO₂ formed under neutral conditions. Almost all the obtained samples are highly effective photocatalysts for water reduction, gas-phase oxidation of alcohol and benzene [61–64].

In the present work, the above approach was used for synthesis of meso-nc-TiO₂ samples of both anatase and various phase compositions (anatase, brookite, rutile), as a combination of two or three phases, using hydrochloric acid (HCl) as a catalyst for hydrolysis of the TiO₂ precursor. All samples were calcined at 500 °C.

2 Materials and methods

2.1 Materials

Titanium tetrabutoxide (IV), dibenzo-18-crown-6 (Sigma-Aldrich), dodecyldi- methylethylammonium bromide (Fluka), HCl acid, n-butanol, NaCl and ethanol (96%) (Him-laborreactiv) were used. Commercial TiO₂ Evonik-P25 (Evonik Corp) was chosen as the standard photocatalyst.

2.2 Synthesis

Samples of meso-nc-TiO₂ with different phase compositions were obtained using the modified sol–gel method described in detail in our works [59, 60]. Dibenzo-18-crown-6 (in the form of the sodium complex [Na(DB18C6)] Cl due to the low solubility of crown ether in butanol (BuOH)) was used as a template in the presence (or in the absence) small additives of the cationic surfactant dodecyldimethylethylammonium bromide (DDMEABr) and/or lanthanum salt. The calculated amounts of reagents were sequentially dissolved in butanol (BuOH). Titanium tetrabutoxide (TBOT) was added dropwise under vigorous stirring. In contrast to the mentioned works, in this work, TBOT was hydrolyzed in an acidic medium using hydrochloric acid as catalyst.

The reaction mixture was left under a glass hood in air at room temperature (without stirring) until gel formation has stopped. HTT was carried out at 175 °C for 24 h. All samples (both treated and untreated hydrothermally) were calcined at 500 °C for 4 h.

Samples obtained under various conditions were designated as T_n and T_nH, where n is the number of the sample and H denotes hydrothermal treatment. The molar ratios of the reaction mixture used for the synthesis are shown in Table 1:

Table 1 Molar ratios of starting reagents, used for meso-nc-TiO₂ synthesis

Sample	La ³⁺	TBOT	[Na(DB18C6)]Cl	DDMEABr	H ₂ O	HCl	BuOH	HTT
T1	–	1.0	0.12	–	3	0.4	78	–
T1H	–	1.0	0.12	–	3	0.4	78	+
T2	–	1.0	0.12	0.02	3	0.4	78	–
T2H	–	1.0	0.12	0.02	3	0.4	78	+
T3	0.01	1.0	0.12	–	3	0.4	78	–
T3H	0.01	1.0	0.12	–	3	0.4	78	+
T4	0.01	1.0	0.12	0.02	3	0.4	117	–
T4H	0.01	1.0	0.12	0.02	3	0.4	117	+
T5	0.01	1.0	0.12	0.02	3	0.4	78	–
T5H	0.01	1.0	0.12	0.02	3	0.4	78	+
T6H	0.01	1.0	0.12	0.02	3	0.4	57	+
T7H	0.01	1.0	0.12	0.02	7	0.7	26	+

2.3 2.3 Characterization

A Dron-3.M diffractometer with Cu K_α ($\lambda = 1.5406 \text{ \AA}$) radiation was used for the X-ray diffraction (XRD) analysis to determine the crystal structure and crystallinity of TiO₂. The average size of TiO₂ crystallites (2R) was estimated from the broadening of the anatase peak at $2\theta = 25.4^\circ$ (101) in XRD-spectra using well-known Scherrer's equation.

The morphology of the samples was observed using transmission electron microscopy (TEM) and scanning electron microscopy (SEM) on a JEOL JEM 1230 and a JEOL JSM 6060 LA microscopes respectively. Energy dispersive X-ray (EDX) analysis were performed with a Tescan Measure 3 microscope, equipped with an Oxford X-max energy-dispersive X-ray assay for 80 mm², for an accelerating voltage of 5–20 kV. Electron diffraction patterns were obtained on a transmission electron microscope Selmi TEM-125K with the accelerating voltage of 100 kV.

In some cases, the samples were pre-treated with an ultra sound disperser UZDN-A (radiation power 130 W) for 5 min.

N₂ adsorption–desorption isotherms were recorded at 77 K using an Autosorb-6 automated gas adsorption analyzer (Quantachrome). Prior to the measurements, samples were degassed at 473 K for 12 h. The specific surface area (S_{BET}) of the samples was determined by the BET method. The average pore size (D_p) was calculated using BJH method. The NLDFT method (cylindrical pore model) was used to calculate the pore size distribution from the desorption branch. The mesopore volume (V_p) was determined using amount of N₂ adsorbed at relative pressure p/p_0 of 0.997.

2.4 Photocatalytic oxidation studies

The photocatalytic activity of the obtained meso-nc-TiO₂ samples was studied in the gas-phase reaction of ethanol oxidation. A 50 mg titanium dioxide sample pressed onto a 1 × 3 cm copper support was put into a 150 cm³ glass reactor, equipped with a magnetic stirrer and membrane for sampling. The required amount of alcohol was introduced into the reactor using a microsyringe. For complete evaporation of the alcohol and adsorption equilibrium establishing, the reactor was kept without irradiation with stirring of the gas mixture for ~ 2 h. The samples were irradiated with the focused light of a DRSh-1000 mercury lamp. A region with $\lambda = 310\text{--}390 \text{ nm}$ was isolated from the radiation spectrum by means of filters. The light intensity was measured using a ferrioxalate actinometer ($I = 5 \text{ \mu mol}$ of quants per min). The concentration of the starting substrate was determined using a CHROM 5 gas chromatograph equipped with a flame ionization detector and a column packed with Porapak Q. The initial oxidation rates were determined using the initial linear region over approximately 30 min of irradiation as the ratio of the change in ethanol concentration in the reactor to the irradiation time.

3 Results and discussion

Samples of meso-nc-TiO₂ with different phase composition were obtained by a simple modification of the previously proposed approach [59] through changing the conditions of TBOT hydrolysis, namely, the transition from a neutral to an acidic environment using a well-known acid catalyst—hydrochloric acid [23, 53, 65]. HCl is the most commonly

used due to the lower electronegativity of the chloride anion compared with others and bonding of the Cl⁻ ion to the Ti atom. HCl promotes the hydrolysis reaction versus the condensation reaction [35] as well as serves as an electrolyte to prevent particle growth or agglomeration through electrostatic repulsion. The main concept of such optimization of the previous approach [59, 60] was to combine the factors: HTT, small additives of surfactant and (or) lanthanum salt, the influence of reagents concentration in the presence of HCl on the phase composition of meso-nc-TiO₂ materials (at the same calcination temperature—500 °C).

Figure 1 shows the diffraction patterns of meso-nc-TiO₂ samples obtained in an acidic medium in the presence of HCl. The phase content of each polymorph was determined by the main diffraction peaks of anatase, rutile and brookite, designated as (101), (110) and (121) reflexes, respectively, using the well-known calculation method [66]. The diffraction patterns of samples T2 and T4 contain weak narrow peaks at 32° and 45.5° (2θ), which can be attributed to NaCl, occluded by the main product during the synthesis [60]. The content of NaCl in the samples

was confirmed by the EDX (Table S1). Calculated from XRD date, size of anatase crystallites in samples under consideration is about 10 nm (see Table 2).

Figures 2 and S1 show the N₂ adsorption-desorption isotherms and pore size distributions for meso-nc-TiO₂ samples. All isotherms belong to type IV IUPAC classification with H1 and H2 hysteresis loops located at relative pressure p/p₀ values higher than 0.6, indicating the formation of mesopores in the obtained samples [67, 68].

Table 2 shows the phase composition and texture characteristics of meso-nc-TiO₂ samples. As can be seen from Figs. 1 and 2, S1 and Table 2, the phase composition and texture characteristics of meso-nc-TiO₂ samples were influenced by DDMEABr surfactant additive, lanthanum salt, and concentration of reagents in the initial reaction mixture during synthesis, as well as the heat treatment regime (HTT before calcination).

The efficiency of crown ether templating activity was improved by addition of minute amounts of surfactant using previously described method [60]. The possible mechanism of the process can be explained by the destructuring effect of the surfactant on the solvation shell

Fig. 1 XRD patterns of meso-nc-TiO₂ samples, obtained in various synthetic conditions. Anatase (JCPDS-PDF card no. 21-1272), rutile (JCPDS-PDF card no. 21-1276), brookite (JCPDS-PDF card no. 29-1360)

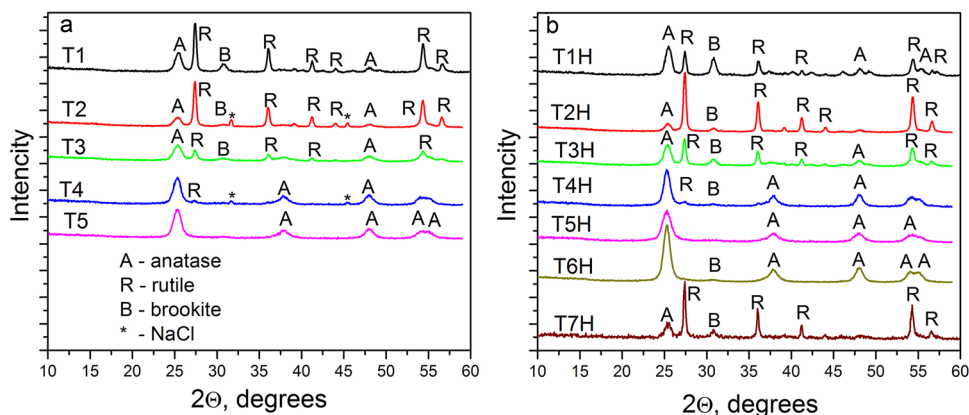
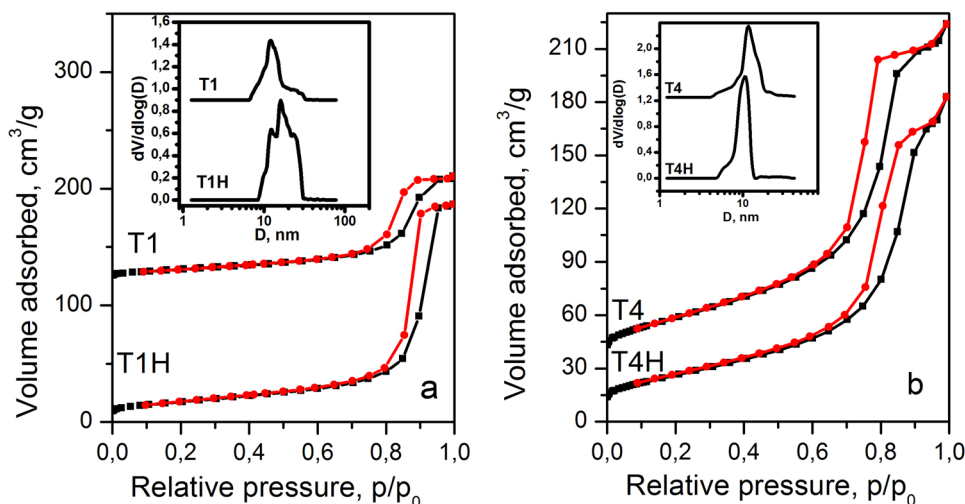


Fig. 2 N₂-adsorption/desorption isotherms and pore size distribution obtained by NLDFT of T1, T1H (a) and T4, T4H samples (b)



of the crown ether complex. "Naked" oxygen atoms from the crown ether can react with structure-forming fragments with Ti to form TiO_2 mesophase framework. As can be seen from Table 2, the addition of DDMEABr lead to the decrease of anatase and brookite content and increase in the content of rutile, respectively (samples T1 and T2). The differences become more visible in a case of HTT processing of these samples (samples T1H and T2H). The presence of a surfactant additive opens possibility for the synthesis of T2H sample with the highest rutile phase content of 70%. The presence of a surfactant lead to a slight increase in the specific surface area (S_{BET}) in the case of calcined samples T1 and T2 (39 m^2/g and 48 m^2/g), on the contrary, for the T1H and T2H samples (with preliminary hydrothermal treatment), there are almost twofold decrease of the corresponding S_{BET} values (61 m^2/g and 33 m^2/g). However, surfactant did not affect the pore diameter of the specified pairs of samples (samples T1–T2 and T1H–T2H) in a great extent.

The addition of lanthanum salt promotes the increase the anatase content and decreases the brookite content regardless of the use of HTT (samples T1, T1H and T3, T3H), while the content of rutile decreases in the absence of HTT (samples T1 and T3) and increases at HTT (samples T1H and T3H). In the case of samples obtained with the simultaneous presence of DDMEABr and lanthanum salt (T1, T1H and T5, T5H, T6H), the three-fold increase of the anatase content is observed along with the a sharp drop of the brookite content and complete disappearance of the rutile phase. The phase composition of the sample undergoes especially profound changes when using HTT (samples T1H and T5H), when the three-phase composition turn into anatase monophase (Fig. 1; Table 2).

Addition of La^{3+} ions to the initial reaction mixture provided a significant increase in the specific surface area. So, for example, for samples T1 and T3, the value of S_{BET} increases twofold (39 m^2/g and 89 m^2/g , respectively). Doping with small amounts of La^{3+} cations was successfully used for thermal stability increasing of mesoporous anatase [60]. The role of this cation in stabilizing the structure of mesoporous TiO_2 has been explained by implantation of rare-earth cations into framework of the oxide system. Lanthanum is more electropositive than titanium and thus formation of the La–O bond causes partial transfer of electrons from the La–O bond to the Ti–O bond leading to strengthening of the latter. La^{3+} does not enter into the crystal lattice of TiO_2 and was uniformly dispersed onto TiO_2 , supported by the results of EDX analysis (Table. S1). The temperature of anatase–rutile transformation significantly increases in the presence of La^{3+} as compared to pure TiO_2 .

Dilution of the initial reaction mixture in the presence of lanthanum salt (samples T3, T3H and T4, T4H, Table 1)

lead to a twofold increase of the anatase content, along with the decrease of the content of brookite and rutile. For example, sample T3 comprises of anatase (55%), rutile (21%) and brookite (24%), and the corresponding sample T4 has only anatase (97%) and rutile (3%) phases. An increase of the concentration of reagents in the initial reaction mixture containing additives of DDMEABr and lanthanum salts (samples T5H, T6H and T7H) allows formation of one, two, and three phase TiO_2 compositions (Fig. 1; Table 2). In the case of sample T7H (compared with samples T5H and T6H), additional amounts of H_2O and HCl, apparently, have a definite effect on the phase composition of this sample.

Upon dilution of the initial reaction mixture in 1.5 times, the specific surface area increases by a factor of ~ 1.5 (samples T3, T3H and T4, T4H), while the pore diameter decreases (samples T3H and T4H). The simultaneous introduction of surfactant additives and La^{3+} ions (samples T5 and T5H) lead to a tremendous increase in the specific surface area S_{BET} of meso-nc- TiO_2 samples compared to samples obtained only in the presence of surfactant (samples T2 and T2H) or La^{3+} ions (samples T3 and T3H).

As follows from a comparison of the texture characteristics of the samples presented in Table 2, the T5H sample has the largest specific surface area ($S_{\text{BET}} = 132 \text{ m}^2/\text{g}$) and pore volume ($V_p = 0.46 \text{ cm}^3/\text{g}$). An increase of the concentration of the starting reagents (samples T5H and T6H) lead to a 1.5-fold decrease in the specific surface and a substantial increase in pore diameter ($\sim 25\%$) with a constant pore volume.

The values of the average sizes of anatase crystallites presented in Table 2 fall in the range of 7.0–10.4 nm, and the highest values are observed for samples T1 (9.8 nm) and T1H (10.4 nm) obtained without DDMEABr or lanthanum salt.

The choice of the heat treatment mode (calcination or calcination with preliminary hydrothermal treatment) significantly affects the phase composition of meso-nc- TiO_2 nanocomposites (samples T1 and T1H, T2 and T2H, T3 and T3H, T4 and T4H, T5 and T5H) in all cases. For example, a T1 sample subjected to calcination only has a composition of anatase (29%), rutile (39%) and brookite (32%), and a T1H sample (preliminary hydrothermally treated)-anatase (34%), rutile (14%) and brookite (52%). It should be noted that among all meso-nc- TiO_2 samples, the T1H sample (obtained in the absence of any additives) contains the highest amount of brookite.

Comparison of the texture characteristics of samples T2 and T2H (obtained in the presence of a surfactant), T3 and T3H, T4 and T4H (obtained in the presence of lanthanum salt), hydrothermal treatment before calcination lead to a decrease in the specific surface ($\sim 20\text{--}30\%$) and a significant increase in pore diameter ($\sim 20\text{--}80\%$) along with

a change in pore volume (an increase of almost 1.5 times) only in the case of the T3H sample (Table 2). In the case of samples T5 and T5H (obtained with the simultaneous presence of La^{3+} ions and a surfactant), on the contrary, the T5H sample previously hydrothermally treated before calcination compared to a simply calcined sample T5 showed an increase in specific surface area (~ 35%) with a

simultaneous increase in ~2.5 times the pore volume and in 2 times the pore diameter.

As follows from the TEM data (Figs. 3, S2–7), all samples of meso-nc-TiO₂ has homogeneous, spherical primary particles (anatase phase). The sizes of anatase crystallites in the samples estimated from TEM are in good agreement with the corresponding values, calculated by

Fig. 3 TEM of T1 (a, b) and T1H (c, d), T4 (e, f) and T4H (g, h)

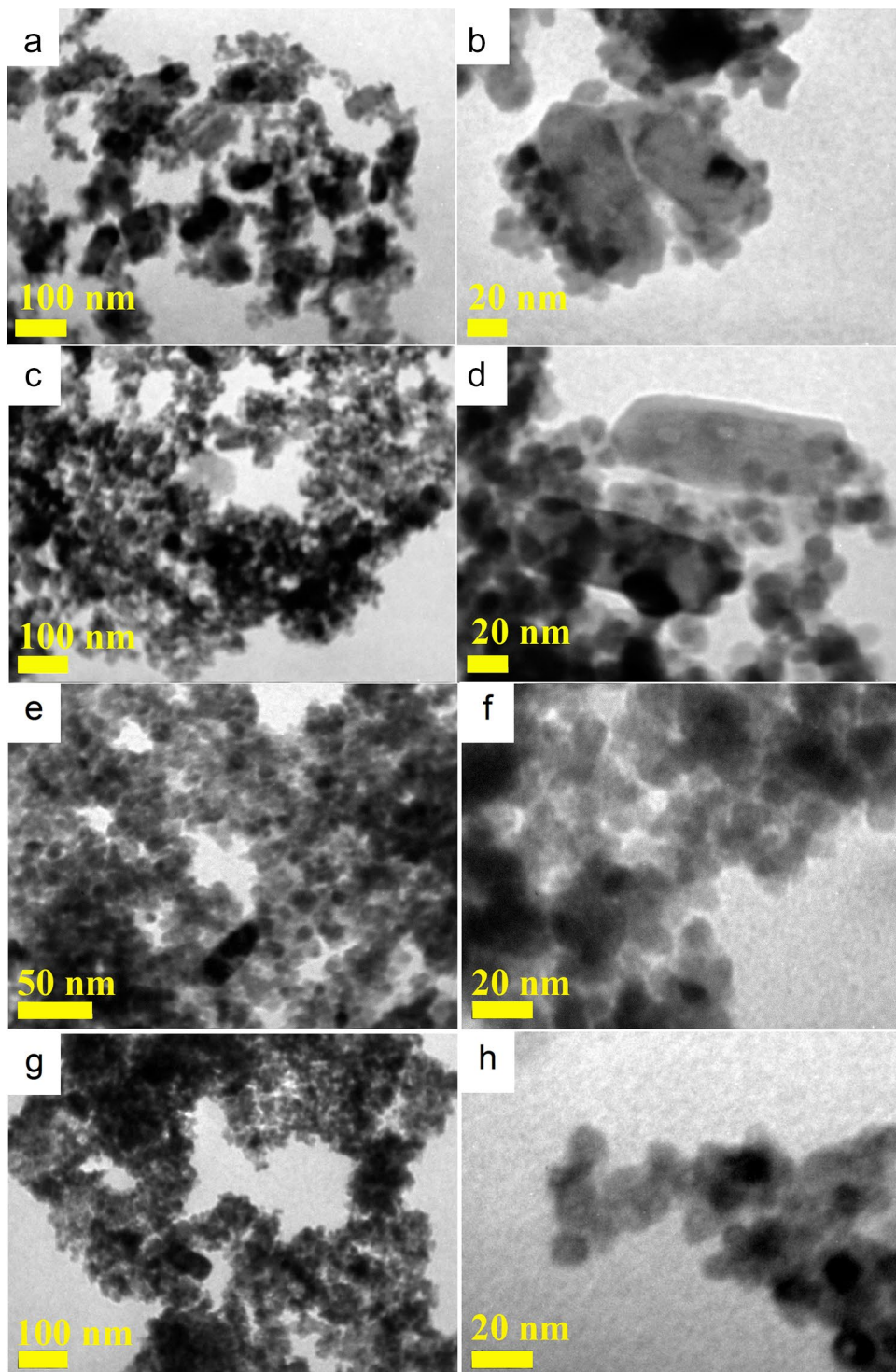


Table 2 Synthesis conditions of meso-nc-TiO₂ samples, their specific surface area (S_{BET}), pore volume (V_p), pore diameter (D_p), crystallite size and phase composition

Sample	Additives		TBOT/BuOH	HTT	S_{BET} , m ² /g	V_p , cm ³ /g	D_p , nm	Crystalline size by XRD, nm	Phase composition		
	DDMEABr	La ³⁺							A	R	B
T1	–	–	1:78	–	39	0.14	14.5	9.8	29	39	32
T1H	–	–	1:78	+	61	0.29	18.9	10.4	34	14	52
T2	+	–	1:78	–	48	0.23	13.0	7.2	22	60	18
T2H	+	–	1:78	+	33	0.21	17.4	9.4	16	70	14
T3	–	+	1:78	–	83	0.21	9.4	7.1	55	21	24
T3H	–	+	1:78	+	64	0.30	17.3	8.2	43	28	29
T4	–	+	1:117	–	122	0.31	9.4	8.3	97	3	–
T4H	–	+	1:117	+	96	0.28	11.3	9.5	85	4	11
T5	+	+	1:78	–	98	0.18	7.0	7.4	88	–	12
T5H	+	+	1:78	+	132	0.46	13.9	7.0	100	–	–
T6H	+	+	1:57	+	90	0.44	17.3	9.1	90	–	10
T7H	+	+	1:26	+	100	0.30	12.3	10.2	25	45	30
P 25	–	–	–	–	50	–	–	25	70	30	–

V_p , total pore volume, D_p , pore diameter, A, anatase, R, rutile, B, brookite

Experiment errors: $S_{\text{BET}} \pm 2\text{--}5$ m²/g, $V_p \pm 0.002\text{--}0.005$ cm³/g, $D_p \pm 0.5\text{--}1$ nm, Crystalline size ± 1 nm

the Scherrer formula (Table 2). Samples in which the percentage of the rutile and brookite phases are high (T1, T1H, T2, T2H, T3, T3H, T7H), shows the presence of crystallites in the form of variously sized plates of hexagons and quadrangles shapes (Fig. 3a–d, Fig. S2–7). Electron diffraction patterns are in good agreement with the XRD (Fig. S8–9).

Figures 4, 5, 6 and 7, S10–18 show SEM images of meso-nc-TiO₂ samples. As follows from Figs. 4, S10–12 there are no microspheres in samples of T1 and T1H, T2 and T2H obtained with and without HTT. Earlier [59–61, 63], we have showed that TiO₂ samples obtained in a similar way under neutral conditions—microscopic particles with a well-defined spherical shape, were mesoporous TiO₂

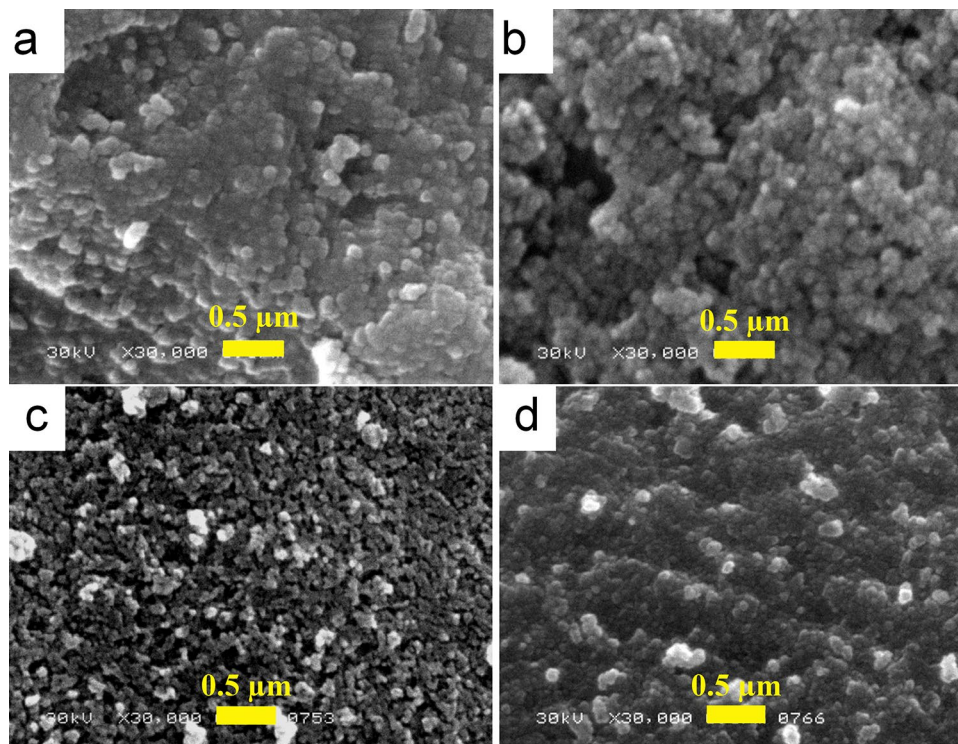
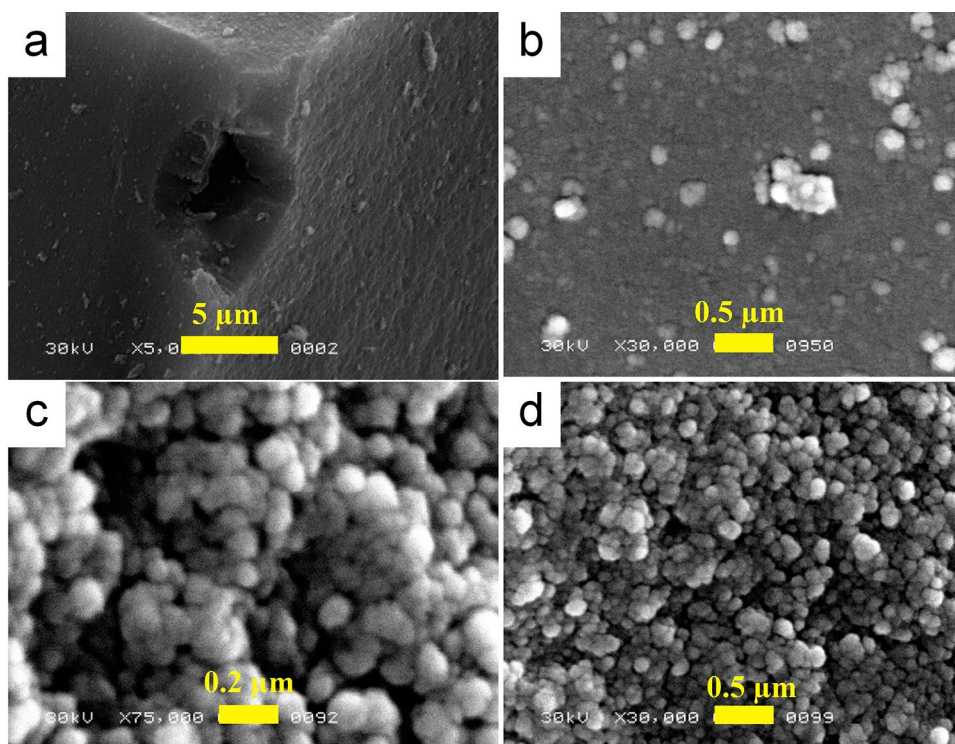
Fig. 4 SEM of T1 (a) and T1H (b-after ultrasonic treatment), T2 (c) and T2H (d)

Fig. 5 SEM of T3 (a, b) and T3H (c, d)



microspheres (1–3 μm), which consist of spherical homogeneous nanoparticles (secondary particles) 30–50 nm in size, which in turn were formed by aggregation of anatase crystallites (primary particles) of about 10 nm in size. This led us to the conclusion that the presence of hydrochloric acid prevented the formation of microspheres. All meso-nc-TiO₂ samples formed in acidic medium were aggregates of various sizes (from 100 to 500 nm). During ultrasonic treatment of samples T1H, T4, T4H, T5H, T6H, the aggregates break up into homogeneous nanoscale (40–100 nm) secondary particles of spherical or spheroidal shape (Figs. 4b, 6a, e, f, 7a, b, S15).

4 Photochemistry

For evaluation of photocatalytic activity of meso-nc-TiO₂ samples, we used the gas-phase oxidation of ethanol as a model process for the oxidation of organic substrates [69–73].

Such an assessment is of particular interest because all titanium polymorph compositions were obtained within the same synthetic method using the same heat treatment mode (calcination at 500 °C) [74–76].

Histograms of the phase composition of meso-nc-TiO₂ samples and the corresponding values of ethanol oxidation initial rates are shown in the Fig. 8a, b. As can be seen, all the samples significantly outperformed the commercial photocatalyst Evonik P25 in photocatalytic activity. The

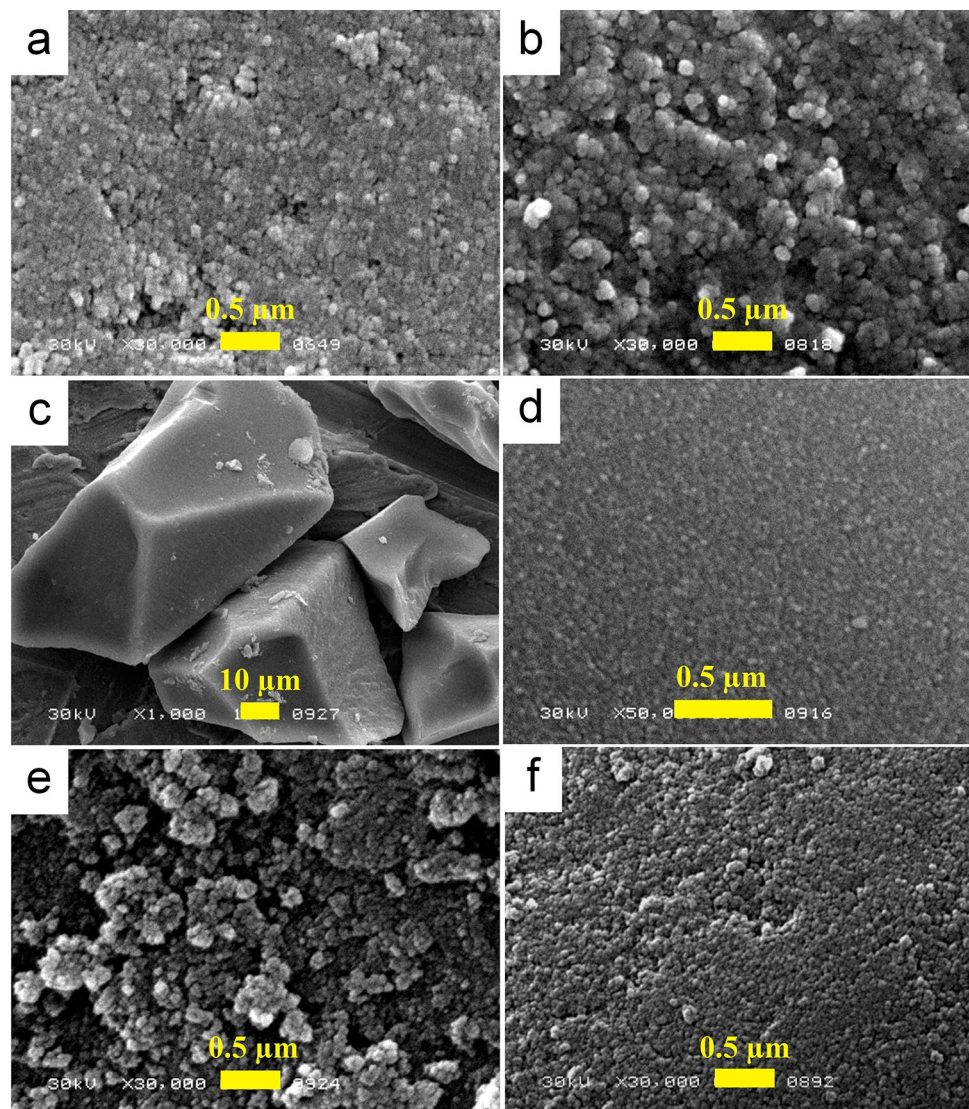
dependence of the photocatalytic activity of the obtained samples, except for T4 and T4H, in the process under study increases almost linearly with an increase in the content of the anatase phase (Fig. 9a). The activity of the T4 and T4H samples is significantly higher than the activity of the meso-nc-TiO₂ samples with similar anatase content (T5, T5H, T6H) (Fig. 9a).

Sample T4 has a composition of anatase (97%)-rutile (3%) phases, and sample T4H-anatase (85%)-rutile (4%)-brookite (11%) phases. The T5H sample (anatase ~ 100%), was noticeably inferior in activity to the T4 and T4H samples. Samples T5 and T6H are very close in composition (88% anatase and 90% anatase, 12% brookite and 10% brookite, respectively), but, unlike the T4 biphasic sample and the T4H three-phase sample, did not contain rutile phase.

Samples T4 and T4H also significantly deviate from the dependence of the photocatalytic activity of samples on their specific surface area (Fig. 9b). In this case, the activity of the T4 and T4H samples is significantly higher than that of the samples with a similar specific surface area (T5, T5H, T7H).

The observed picture can apparently be explained by the synergistic effect [16, 19, 77] due to the combination of the anatase and rutile phases in the phase compositions of T4 (anatase (97%)-rutile (3%)) and T4H (anatase (85%)-rutile (4%)-brookite (11%)). The authors of [77] have showed that even 2% content of rutile in

Fig. 6 SEM of T4 (a-after ultrasonic treatment) and T4H (b), T5 (c, d) и T5H (e, f-after ultrasonic treatment)



anatase-rutile mixed-phase promotes the photocatalytic activity of TiO_2 . A significant increase in the photocatalytic activity of anatase composites with a small amount of rutile can be associated with the different positions of the energy levels in anatase and rutile [78], which leads to spatial separation of photogenerated charges between the components of the composite and a decrease in the unwanted electron-hole recombination (Fig. S19). In the case of composites of anatase with brookite, the synergistic effect is not observed, which is associated with a higher level of the conduction band of brookite compared to anatase [78] and the absence of separation of charges photogenerated in anatase between the components of the composite (Fig. S19). In other samples obtained containing rutile, the positive effect of charge separation is compensated by the relatively low content of the active phase of anatase.

5 Conclusions

Binary and ternary phase mixtures of mesoporous nanocrystalline titanium dioxide samples with different phase composition and texture were obtained by sol-gel synthesis (with or without hydrothermal treatment). The anatase phase, the content of which in the samples ranged from 16 to ~100%, consisted of homogeneous spherical anatase crystallites ~10 nm in size.

The phase composition of the meso-nc- TiO_2 samples was formed by varying the concentrations of the reagents, using small additions of dodecyldimethylammonium bromide surfactant and/or lanthanum salt in the reaction mixture and hydrothermal treatment. All synthesized samples were calcined at the same temperature of 500 °C for 4 h. This is the crucial condition for formation a number of photocatalysts with different phase composition for a comparative assessment of their photocatalytic activity.

Fig. 7 SEM of T6H (a, b-after ultrasonic treatment) and T7H (c, d)

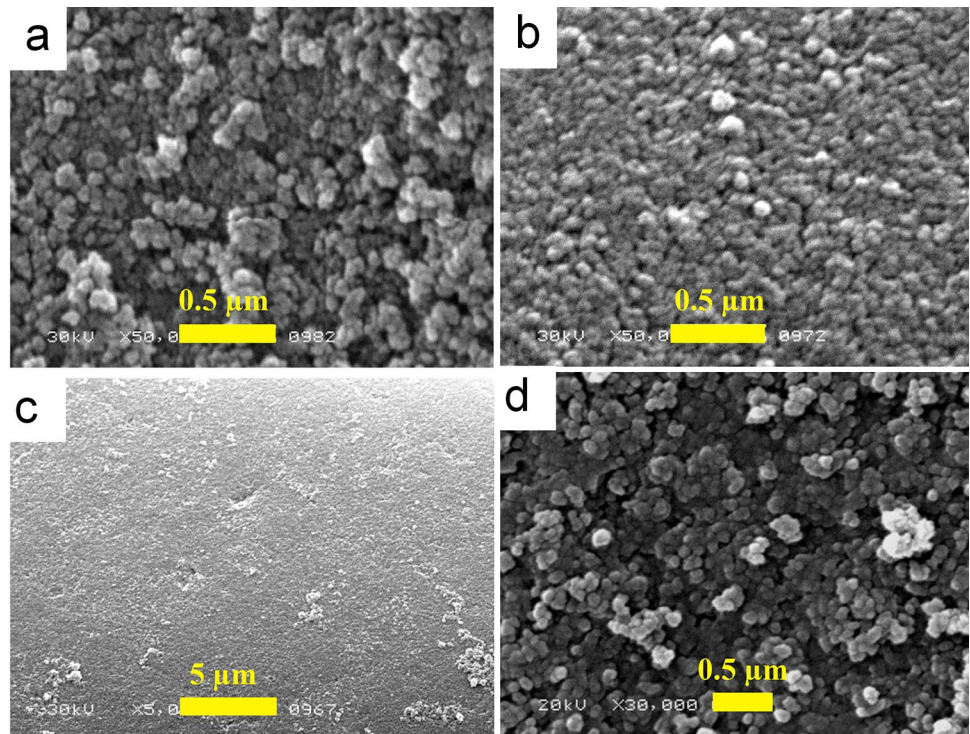


Fig. 8 Phase composition (a) and the corresponding ethanol oxidation initial rates (b) of meso-nc-TiO₂ samples

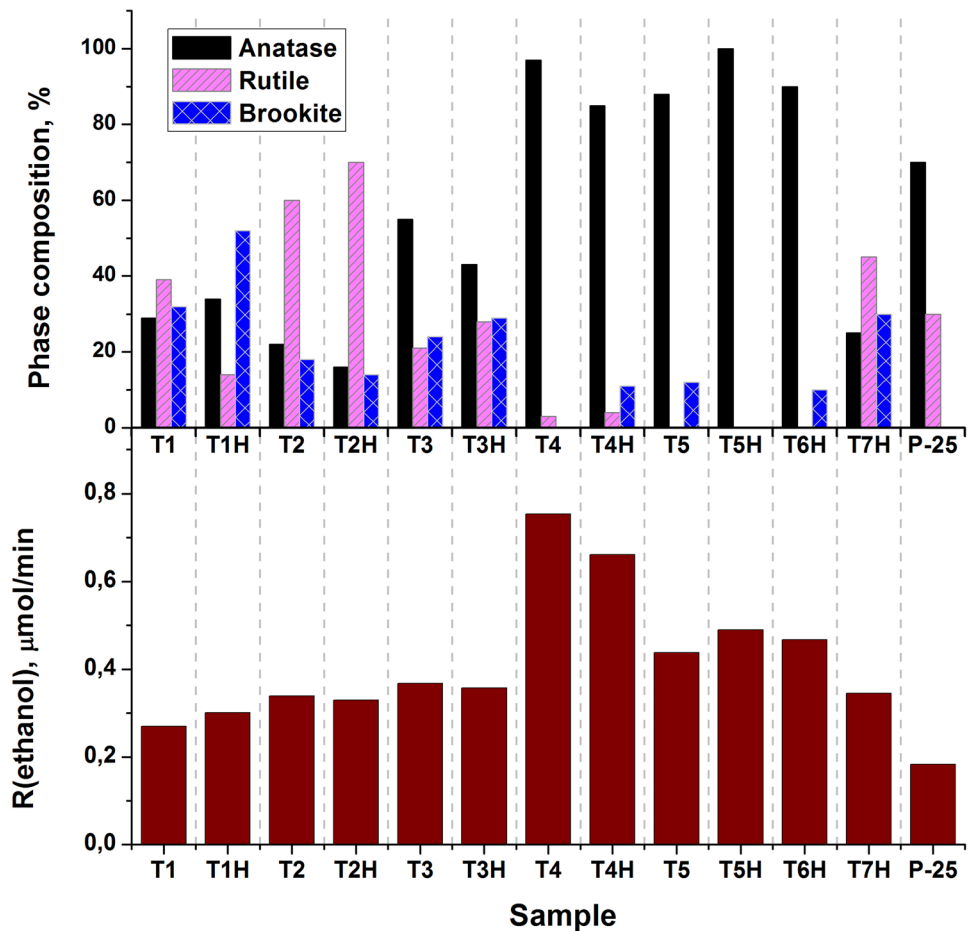
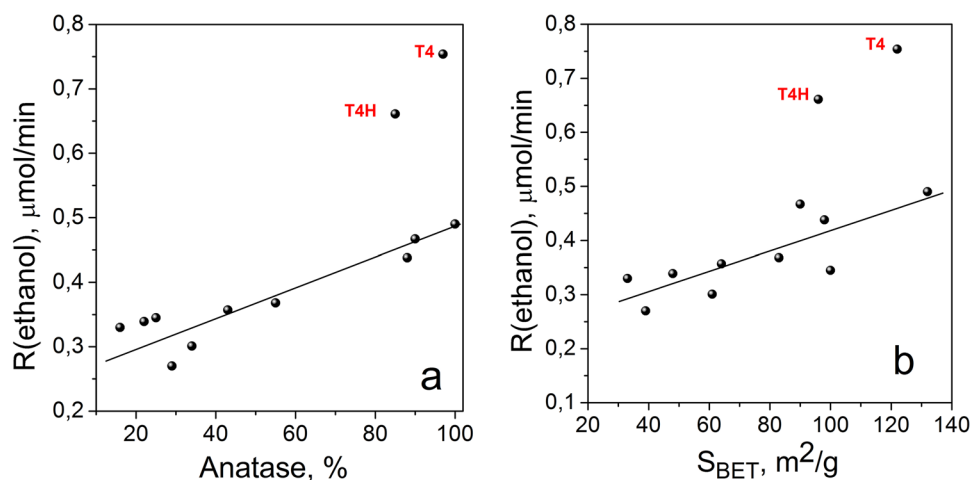


Fig. 9 The dependence of the ethanol oxidation initial rates in the presence of meso-nc-TiO₂ samples upon anatase content (a) and S_{BET} (b)



Meso-nc-TiO₂ samples with anatase content over 80% had the high level of photoactivity. The highest photocatalytic activity was demonstrated by the sample with an anatase phase (97%)-rutile (3%) composition.

Acknowledgements This research was supported by the General Research Project of the L.V. Pisarzhevskii Institute of Physical Chemistry NAS of Ukraine (funded by the National Academy of Sciences of Ukraine).

Declaration

Conflict of interest On behalf of all authors, the corresponding author states that there is no conflict of interest.

Open Access This article is licensed under a Creative Commons Attribution 4.0 International License, which permits use, sharing, adaptation, distribution and reproduction in any medium or format, as long as you give appropriate credit to the original author(s) and the source, provide a link to the Creative Commons licence, and indicate if changes were made. The images or other third party material in this article are included in the article's Creative Commons licence, unless indicated otherwise in a credit line to the material. If material is not included in the article's Creative Commons licence and your intended use is not permitted by statutory regulation or exceeds the permitted use, you will need to obtain permission directly from the copyright holder. To view a copy of this licence, visit <http://creativecommons.org/licenses/by/4.0/>.

References

- Chen X, Mao SS (2007) Titanium dioxide nanomaterials: synthesis, properties, modifications, and applications. *Chem Rev* 107(7):2891–2959. <https://doi.org/10.1021/cr0500535>
- Nakata K, Fujishima A (2012) TiO₂ photocatalysis: design and applications. *J Photochem Photobiol C Photochem Rev* 13(3):169–189. <https://doi.org/10.1016/j.jphotochemrev.2012.06.001>
- Soler-Illia GJ, de AA, Sanchez, Lebeau C, Patarin B J (2002) Chemical strategies to design textured materials: from microporous and mesoporous oxides to nanonetworks and hierarchical structures. *Chem Rev* 102(11):4093–4138. <https://doi.org/10.1021/cr0200062>
- Pelaez M, Nolan NT, Pillai SC, Seery MK, Falaras P, Kontos AG, Dunlop PSM, Hamilton JJJ, Byrne JA, O'Shea K, Entezari MH, Dionysiou DD (2012) A review on the visible light active titanium dioxide photocatalysts for environmental applications. *Appl Catal B Environ* 125:331–349. <https://doi.org/10.1016/j.apcatb.2012.05.036>
- Hagfeldt A, Graetzel M (1995) Light-induced redox reactions in nanocrystalline systems. *Chem Rev* 95(1):49–68. <https://doi.org/10.1021/cr00033a003>
- Tong H, Ouyang S, Bi Y, Umezawa N, Oshikiri M, Ye J (2012) Nanophotocatalytic materials: possibilities and challenges. *Adv Mater* 24(2):229–251. <https://doi.org/10.1002/adma.201102752>
- Fresno F, Portela R, Suárez S, Coronado JM (2014) Photocatalytic materials: recent achievements and near future trends. *J Mater Chem A* 2(9):2863–2884. <https://doi.org/10.1039/C3TA13793G>
- Wang Y, Sun C, Zhao X, Cui B, Zeng Z, Wang A, Liu G, Cui H (2016) The application of nano-TiO₂ photo semiconductors in agriculture. *Nanoscale Res Lett* 11(1):529. <https://doi.org/10.1186/s11671-016-1721-1>
- Kumar N, Chauhan NS, Mittal A, Sharma S (2018) TiO₂ and its composites as promising biomaterials: a review. *Biometals* 31(2):147–159. <https://doi.org/10.1007/s10534-018-0078-6>
- Macwan DP, Dave PN, Chaturvedi S (2011) A review on nano-TiO₂ sol-gel type syntheses and its applications. *J Mater Sci* 46(11):3669–3686. <https://doi.org/10.1007/s10853-011-5378-y>
- Noman MT, Ashraf MA, Ali A (2019) Synthesis and applications of nano-TiO₂: a review. *Environ Sci Pollut Res* 26(4):3262–3291. <https://doi.org/10.1007/s11356-018-3884-z>
- Humayun M, Raziq F, Khan A, Luo W (2018) Modification strategies of TiO₂ for potential applications in photocatalysis: a critical review. *Green Chem Lett Rev* 11(2):86–102. <https://doi.org/10.1080/17518253.2018.1440324>
- Zhang W, Zou L, Wang L (2009) Photocatalytic TiO₂/adsorbent nanocomposites prepared via wet chemical impregnation for wastewater treatment: a review. *Appl Catal A Gen* 371(1–2):1–9. <https://doi.org/10.1016/j.apcata.2009.09.038>
- Verma R, Gangwar J, Srivastava AK (2017) Multiphase TiO₂ nanostructures: a review of efficient synthesis, growth mechanism, probing capabilities, and applications in bio-safety and health. *RSC Adv* 7(70):44199–44224. <https://doi.org/10.1039/C7RA06925A>
- Etacheri V, Di Valentin C, Schneider J, Bahnemann D, Pillai SC (2015) Visible-light activation of TiO₂ photocatalysts: Advances in theory and experiments. *J Photochem Photobiol C Photochem Rev* 25:1–29. <https://doi.org/10.1016/j.jphotochemrev.2015.08.003>

16. Bagheri S, Julkapli NM (2017) Mixed-phase TiO₂ photocatalysis: correlation between phase composition and photodecomposition of water pollutants. *Rev Inorg Chem* 37(1):11–28. <https://doi.org/10.1515/revic-2016-0001>
17. Deng X, Wang Y, Chen Y, Cui Z, Shi C (2019) Yttrium-doped TiO₂ compact layers for efficient perovskite solar cells. *J Solid State Chem* 275:206–209. <https://doi.org/10.1016/j.jssc.2019.04.022>
18. Wen J, Xie J, Chen X, Li X (2017) A review on g-C₃N₄-based photocatalysts. *Appl Surf Sci* 391:72–123. <https://doi.org/10.1016/j.apsusc.2016.07.030>
19. Paul KK, Giri PK (2018) Shape tailored TiO₂ nanostructures and their hybrids for advanced energy and environmental applications: a review. *J Nanosci Nanotechnol* 19(1):307–331. <https://doi.org/10.1166/jnn.2019.15778>
20. Luo Z, Poyraz AS, Kuo C-H, Miao R, Meng Y, Chen S-Y, Jiang T, Wenos C, Suib SL (2015) Crystalline mixed phase (anatase/rutile) mesoporous titanium dioxides for visible light photocatalytic activity. *Chem Mater* 27(1):6–17. <https://doi.org/10.1021/cm5035112>
21. Qiu Y, Ouyang F, Zhu R (2017) A facile nonaqueous route for preparing mixed-phase TiO₂ with high activity in photocatalytic hydrogen generation. *Int J Hydrog Energy* 42(16):11364–11371. <https://doi.org/10.1016/j.ijhydene.2017.03.047>
22. Chang JA, Vital M, Baek IC, Seok S, Il (2009) Morphological and phase evolution of TiO₂ nanocrystals prepared from peroxotitanate complex aqueous solution: influence of acetic acid. *J Solid State Chem* 182(4):749–756. <https://doi.org/10.1016/j.jssc.2008.12.024>
23. Cano-Casanova L, Amorós-Pérez A, Lillo-Ródenas M, Román-Martínez M (2018) Effect of the preparation method (sol–gel or hydrothermal) and conditions on the TiO₂ properties and activity for propene oxidation. *Materials (Basel)* 11(11):2227. <https://doi.org/10.3390/ma11112227>
24. Di Paola A, Bellardita M, Palmisano L (2013) Brookite, the least known TiO₂ photocatalyst. *Catalysts* 3(1):36–73. <https://doi.org/10.3390/catal3010036>
25. Brinker CJ, Scherer GW (1990) Sol–gel science: the physics and chemistry of sol–gel processing. Academic Press, Boston. <https://doi.org/10.1002/adma.19910031025>
26. Antonelli DM, Ying JY (1995) Synthesis of hexagonally packed mesoporous TiO₂ by a modified sol–gel method. *Angew Chemie Int Ed English* 34(18):2014–2017. <https://doi.org/10.1002/anie.199520141>
27. Yang P, Zhao D, Margolese DI, Chmelka BF, Stucky GD (1998) Generalized syntheses of large-pore mesoporous metal oxides with semicrystalline frameworks. *Nature* 396(6707):152–155. <https://doi.org/10.1038/24132>
28. Ismail AA, Bahnemann DW (2011) Mesoporous titania photocatalysts: preparation, characterization and reaction mechanisms. *J Mater Chem* 21(32):11686. <https://doi.org/10.1039/c1jm10407a>
29. Chen L-H, Li X-Y, Deng Z, Hu Z-Y, Rooke JC, Krief A, Yang X-Y, Su B-L (2013) Hydrothermal and surfactant treatment to enhance the photocatalytic activity of hierarchically meso–macroporous titanias. *Catal Today* 212:89–97. <https://doi.org/10.1016/j.cattod.2012.07.021>
30. Hung I-M, Wang Y, Huang C-F, Fan Y-S, Han Y-J, Peng H-W (2010) Effects of templating surfactant concentrations on the mesostructure of ordered mesoporous anatase TiO₂ by an evaporation-induced self-assembly method. *J Eur Ceram Soc* 30(10):2065–2072. <https://doi.org/10.1016/j.jeurceramsoc.2010.04.015>
31. Shen X, Tian B, Zhang J (2013) Tailored preparation of titania with controllable phases of anatase and brookite by an alkaline hydrothermal route. *Catal Today* 201:151–158. <https://doi.org/10.1016/j.cattod.2012.04.038>
32. Mohamed MA, Wan Salleh WN, Jaafar J, Yusof N (2014) Preparation and photocatalytic activity of mixed phase anatase/rutile TiO₂ nanoparticles for phenol degradation. *J Teknol (Sciences Eng)* 70(2):65–70. <https://doi.org/10.11113/jt.v70.3437>
33. Wu M, Lin G, Chen D, Wang G, He D, Feng S, Xu R (2002) Sol-hydrothermal synthesis and hydrothermally structural evolution of nanocrystal titanium dioxide. *Chem Mater* 14(5):1974–1980. <https://doi.org/10.1021/cm0102739>
34. Yang X, Konishi H, Xu H, Wu M (2006) Comparative Sol–hydro(solvo)thermal synthesis of TiO₂ nanocrystals. *Eur J Inorg Chem* 2006(11):2229–2235. <https://doi.org/10.1002/ejic.20050855>
35. Wang C-C, Ying JY (1999) Sol–gel synthesis and hydrothermal processing of anatase and rutile titania nanocrystals. *Chem Mater* 11(11):3113–3120. <https://doi.org/10.1021/cm990180f>
36. Castrejón-Sánchez V, López R, Ramón-González M, Enríquez-Pérez Á, Camacho-López M, Villa-Sánchez G (2018) Annealing control on the anatase/rutile ratio of nanostructured titanium dioxide obtained by sol–gel. *Crystals* 9(1):22. <https://doi.org/10.3390/cryst9010022>
37. Kumar A (2018) Different methods used for the synthesis of TiO₂ based nanomaterials: a review. *Am J Nano Res Appl* 6(1):1. <https://doi.org/10.11648/j.nano.20180601.11>
38. Bamne J, Sharma PK, Haque FZ (2018) Effect of solvent mixing and calcination temperature on the growth of TiO₂ nanoparticles prepared via sol–gel method. *Mater Focus* 7(2):232–241. <https://doi.org/10.1166/mat.2018.1502>
39. Carrera-López R, Castillo-Cervantes S (2012) Effect of the phase composition and crystallite size of sol–gel TiO₂ nanoparticles on the acetaldehyde photodecomposition. *Superf y Vacío* 25(2):82–87
40. Sheikhejad-Bishe O, Zhao F, Rajabtabar-Darvishi A, Khodadad E, Mostofizadeh A, Huang Y (2014) Influence of temperature and surfactant on the photocatalytic performance of TiO₂ Nanoparticles. *Int J Electrochem Sci* 9(8):4230–4240
41. Masolo E, Meloni M, Garroni S, Mulas G, Enzo S, Baró M, Rossinyol E, Rzeszutek A, Herrmann-Geppert I, Pilo M (2014) Mesoporous titania powders: the role of precursors, ligand addition and calcination rate on their morphology, crystalline structure and photocatalytic activity. *Nanomaterials* 4(3):583–598. <https://doi.org/10.3390/nano4030583>
42. Yue Y, Gao Z (2000) Synthesis of mesoporous TiO₂ with a crystalline framework. *Chem Commun* 18:1755–1756. <https://doi.org/10.1039/b004124f>
43. Byrappa K, Adschiri T (2007) Hydrothermal technology for nanotechnology. *Prog Cryst Growth Charact Mater* 53(2):117–166. <https://doi.org/10.1016/j.pcrysgrow.2007.04.001>
44. Luís AM, Neves MC, Mendonça MH, Monteiro OC (2011) Influence of calcination parameters on the TiO₂ photocatalytic properties. *Mater Chem Phys* 125(1–2):20–25. <https://doi.org/10.1016/j.matchemphys.2010.08.019>
45. Agarwala P, Makkar P, Sharma S, Garg R (2014) The effect of heat treatment of TiO₂ nanoparticles on photovoltaic performance of fabricated DSSCs. *J Mater Eng Perform* 23(10):3703–3709. <https://doi.org/10.1007/s11665-014-1131-4>
46. Yu JC, Yu J, Zhang L, Ho W (2002) Enhancing effects of water content and ultrasonic irradiation on the photocatalytic activity of nano-sized TiO₂ powders. *J Photochem Photobiol A Chem* 148(1–3):263–271. [https://doi.org/10.1016/S1010-6030\(02\)00052-7](https://doi.org/10.1016/S1010-6030(02)00052-7)
47. Pulido Melián E, González Díaz O, Doña Rodríguez JM, Colón G, Navío JA, Pérez Peña J (2012) Effect of hydrothermal treatment on structural and photocatalytic properties of TiO₂ synthesized by sol–gel method. *Appl Catal A Gen* 411–412:153–159. <https://doi.org/10.1016/j.apcata.2011.10.033>

48. Luttrell T, Halpegamage S, Tao J, Kramer A, Sutter E, Batzill M (2015) Why is anatase a better photocatalyst than rutile? Model studies on epitaxial TiO₂ films. *Sci Rep* 4(1):4043. <https://doi.org/10.1038/srep04043>
49. Lei J, Li H, Zhang J, Anpo M (2016) mixed-phase TiO₂ nano-materials as efficient photocatalysts. In: Ünlü H, Horing NJM, Dabowski J (eds) *Low-dimensional and nanostructured materials and devices*. NanoScience and Technology. Springer, Cham. https://doi.org/10.1007/978-3-319-25340-4_17
50. Fischer K, Gawel A, Rosen D, Krause M, Abdul Latif A, Griebel J, Prager A, Schulze A (2017) Low-temperature synthesis of anatase/rutile/brookite TiO₂ nanoparticles on a polymer membrane for photocatalysis. *Catalysts* 7(7):209. <https://doi.org/10.3390/catal7070209>
51. Mahshid S, Askari M, Sasani Ghamsari M, Afshar N, Lahuti S (2009) Mixed-phase TiO₂ nanoparticles preparation using sol-gel method. *J Alloys Compd* 478(1–2):586–589. <https://doi.org/10.1016/j.jallcom.2008.11.094>
52. Connelly K, Wahab AK, Idriss H (2012) Photoreaction of Au/TiO₂ for hydrogen production from renewables: a review on the synergistic effect between anatase and rutile phases of TiO₂. *Mater Renew Sustain Energy* 1(1):3. <https://doi.org/10.1007/s40243-012-0003-9>
53. Kaplan R, Erjavec B, Dražić G, Grdadolnik J, Pintar A (2016) Simple synthesis of anatase/rutile/brookite TiO₂ nanocomposite with superior mineralization potential for photocatalytic degradation of water pollutants. *Appl Catal B Environ* 181:465–474. <https://doi.org/10.1016/j.apcatb.2015.08.027>
54. Baghernejhad B (2016) Nano-TiO₂: an efficient and useful catalyst for the synthesis of 3-acetyl- coumarin derivatives. *Res J Pharm Biol Chem Sci* 7(2):1248
55. Kumar SG, Devi LG (2011) Review on modified TiO₂ photocatalysis under UV/visible light: selected results and related mechanisms on interfacial charge carrier transfer dynamics. *J Phys Chem A* 115(46):13211–13241. <https://doi.org/10.1021/jp204364a>
56. Boppella R, Basak P, Manorama SV (2012) Viable method for the synthesis of biphasic TiO₂ nanocrystals with tunable phase composition and enabled visible-light photocatalytic performance. *ACS Appl Mater Interfaces* 4(3):1239–1246. <https://doi.org/10.1021/am201354r>
57. Boehme M, Ensinger W (2011) Mixed phase anatase/rutile titanium dioxide nanotubes for enhanced photocatalytic degradation of methylene-blue. *Nano-Micro Lett* 3(4):236–241. <https://doi.org/10.1007/bf03353678>
58. Mutuma BK, Shao GN, Kim WD, Kim HT (2015) Sol-gel synthesis of mesoporous anatase-brookite and anatase-brookite-rutile TiO₂ nanoparticles and their photocatalytic properties. *J Colloid Interface Sci* 442:1–7. <https://doi.org/10.1016/j.jcis.2014.11.060>
59. Ermokhina NI, Nevinskiy VA, Manorik PA, Ilyin VG, Shcherbatyuk NN, Klymchuk DO, Puziy AM (2012) Synthesis of large-pore mesoporous nanocrystalline TiO₂ microspheres. *Mater Lett* 75:68–70. <https://doi.org/10.1016/j.matlet.2012.01.133>
60. Ermokhina NI, Nevinskiy VA, Manorik PA, Ilyin VG, Novichenko VN, Shcherbatyuk MM, Klymchuk DO, Tsyba MM, Puziy AM (2013) Synthesis and characterization of thermally stable large-pore mesoporous nanocrystalline anatase. *J Solid State Chem* 200:90–98. <https://doi.org/10.1016/j.jssc.2012.12.034>
61. Stroyuk OL, Ermokhina NI, Korzhak GV, Andryushina NS, Shvalagin VV, Kozytskiy AV, Manoryk PA, Barakov RY, Kuchmiy SY, Shcherbatyuk M, Sapsay VI, Puziy AM (2017) Photocatalytic and photoelectrochemical properties of hierarchical mesoporous TiO₂ microspheres produced using a crown template. *J Photochem Photobiol A Chem* 334:26–35. <https://doi.org/10.1016/j.jphotochem.2016.10.039>
62. Stroyuk AL, Ermokhina NI, Korzhak AV, Andryushina NS, Kozytskiy AV, Manorik PA, Ilyin VG, Puziy AM, Sapsay VI, Shcherbatyuk NN (2015) Photocatalytic and photoelectrochemical characteristics of mesoporous titanium dioxide microspheres. *Theor Exp Chem* 51(3):183–190. <https://doi.org/10.1007/s11237-015-9414-x>
63. Shvalagin V, Ermokhina N, Romanovska N, Barakov R, Manorik P, Sapsay V, Shcherbakov S, Poddubnaya O, Puziy A (2019) Mesoporous TiO₂ microspheres with improved efficiency for photooxidation of volatile organic compounds. *Res Chem Intermed* 45(8):4133–4148. <https://doi.org/10.1007/s11164-019-03896-z>
64. Ermokhina NI, Shvalagin VV, Romanovska NI, Sydorova NA, Manoryk PA, Barakov RY, Shcherbatyuk MM, Klymchuk DO, Puziy AM (2018) Photocatalytic activity of mesoporous titanium dioxide stabilized with lanthanum in the gas-phase oxidation of ethanol. *Theor Exp Chem* 53(6):395–401. <https://doi.org/10.1007/s11237-018-9537-y>
65. Zhou J, Song B, Zhao G, Han G (2012) Effects of acid on the microstructures and properties of three-dimensional TiO₂ hierarchical structures by solvothermal method. *Nanoscale Res Lett* 7(1):217. <https://doi.org/10.1186/1556-276X-7-217>
66. Zhang H, Banfield JF (2000) Understanding polymorphic phase transformation behavior during growth of nanocrystalline aggregates: insights from TiO₂. *J Phys Chem B* 104(15):3481–3487. <https://doi.org/10.1021/jp000499j>
67. Gregg SJ, Sing KSW (1982) Adsorption, surface area and porosity. 2. Auflage. Academic Press, London. <https://doi.org/10.1002/bbpc.19820861019>
68. Kruk M, Jaroniec M (2001) Gas adsorption characterization of ordered organic-inorganic nanocomposite materials. *Chem Mater* 13(10):3169–3183. <https://doi.org/10.1021/cm0101069>
69. Bianchi CL, Pirola C, Galli F, Stucchi M, Morandi S, Cerrato G, Capucci V (2015) Nano and micro-TiO₂ for the photodegradation of ethanol: experimental data and kinetic modelling. *RSC Adv* 5(66):53419–53425. <https://doi.org/10.1039/C5RA05385D>
70. Dionysiou DD, Puma GLi, Ye J, Schneider J, Bahnemann D (2016) Photocatalysis: applications. Royal Society of Chemistry, Cambridge. <https://doi.org/10.1039/9781782627104>
71. Schneider J, Matsuoka M, Takeuchi M, Zhang J, Horiuchi Y, Anpo M, Bahnemann DW (2014) Understanding TiO₂ photocatalysis: mechanisms and materials. *Chem Rev* 114(19):9919–9986. <https://doi.org/10.1021/cr5001892>
72. Anpo M, Kamat PV (2010) Environmentally benign photocatalysts. Springer, New York. <https://doi.org/10.1007/978-0-387-48444-0>
73. Shayegan Z, Lee C-S, Haghghat F (2018) TiO₂ photocatalyst for removal of volatile organic compounds in gas phase: a review. *Chem Eng J* 334:2408–2439. <https://doi.org/10.1016/j.cej.2017.09.153>
74. Hoque M, Guzman M (2018) Photocatalytic activity: experimental features to report in heterogeneous photocatalysis. *Materials (Basel)* 11(10):1990. <https://doi.org/10.3390/ma11101990>
75. Wu M, Long J, Huang A, Luo Y, Feng S, Xu R (1999) Microemulsion-mediated hydrothermal synthesis and characterization of nanosize rutile and anatase particles. *Langmuir* 15(26):8822–8825. <https://doi.org/10.1021/la990514f>
76. Andersson M, Österlund L, Ljungström S, Palmqvist A (2002) Preparation of nanosize anatase and rutile TiO₂ by hydrothermal treatment of microemulsions and their activity for photocatalytic wet oxidation of phenol. *J Phys Chem B* 106(41):10674–10679. <https://doi.org/10.1021/jp025715y>
77. Tobaldi DM, Lajaunie L, Rozman N, Caetano APF, Seabra MP, Sever Škapin A, Arenal R, Labrincha JA (2019) Impact of the absolute rutile fraction on TiO₂ visible-light absorption and visible-light-promoted photocatalytic activity. *J Photochem*

Photobiol A Chem 382:111940. <https://doi.org/10.1016/j.jphotochem.2019.111940>

78. Schneider J, Bahnemann D, Ye J, Puma, GLi, Dionysiou DD (2016) Photocatalysis: fundamentals and perspectives. Royal Society of Chemistry, Cambridge. <https://doi.org/10.1039/9781782622338>

Publisher's note Springer Nature remains neutral with regard to jurisdictional claims in published maps and institutional affiliations.